The Influences of Biomass Burning during TRACE-P Experiment Identified by the Regional Chemical Transport Model

Youhua Tang[1], Gregory R. Carmichael[1], Jung-Hun Woo[1], Narisara Thongboonchoo[1], Gakuji Kurata[2], Itsushi Uno[3], David G. Street[4], Donald R. Blake[5], Rodney J. Weber[6], Robert W. Talbot[7], Yutaka Kondo[8] and Hanwant B. Singh[9]

1 Center for Global and Regional Environmental Research, University of Iowa, Iowa, USA
2 Department of Ecological Engineering, Toyohashi University of Technology, Toyohashi, Japan
3 Research Institute for Applied Mechanics, Kyushu University, Fukuoka, Japan
4 Argonne National Laboratory, Illinois, USA
5 Department of Chemistry, University of California at Irvine, California, USA
6 Georgia Institute of Technology, Georgia, USA
7 Institute for the Study of Earth, Oceans, and Space, University of New Hampshire, New Hampshire, USA
8 Research Center for Advanced Science and Technology, University of Tokyo, Tokyo, Japan
9 NASA Ames Research Center, California, USA

Abstract:

Using a regional chemical transport model, STEM 2K1, and the emission inventory for TRACE-P period (Woo et al this issue; Streets et al, this issue), we successfully simulated important features of the biomass CO outflow. Simulated results agree well with the TRACE-P aircraft measurements and Thailand surface observations. Based on sensitivity studies with and without biomass emissions, we identified 9 flight segments that are affected by biomass plumes during TRACE-P period, and compared the characteristics of the biomass airmasses with the other airmasses. The biomass airmasses emitted from Southeast Asia contain relatively high HCN ($\Delta HCN/\Delta CO \sim 0.0015$) and potassium ($\Delta K^+/\Delta CO \sim 0.0038$), but very low NO_y ($\Delta NO_y/\Delta CO \sim 0.005$) mixing ratios, which may be associated with the special burning condition in this region. The biomass airmasses have extreme high ozone production efficiency. The observed $\Delta O_3/\Delta NO_z$ values were ~ 17 in biomass events, and 1.7 in other events. The biomass influence on the trace gas distributions can be divided into two categories: the influence through direct reactions; and the influence caused by biomass aerosols changing J-values. These two influences are discussed for the biomass-affected TRACE-P flights and for East Asia. The biomass influences on chemical species are not only determined by the biomass plume intensity, but also by the ambient environment caused by other emissions. In Southeast Asia, where the biogenic emissions are very strong, the OH background

concentration is low, and the biomass gas-phase compounds mainly contribute to OH production. Arranged in the sensitivity to the J-value change caused by biomass aerosols, we have OH > HO_2 > HCHO > O_3 when evaluated on a regional average. Averaged over March, the biomass burning net influence is as high as 50% for OH, 40% for HO_2, 60% for HCHO, and 10 ppbv for O_3 for the layers below 1km.

KEY WORDS: Biomass Burning; Chemical Transport Model; TRACE-P; Photochemical Process; Aerosols; Radiative influence

INDEX TERMS: 0305 Aerosols and particles; 0322 Constituent sources and sinks; 0345 Pollution—urban and regional; 0365 Troposphere—composition and chemistry; 3337 Numerical modeling and data assimilation; 3359 Radiative processes

1. Introduction:

It is widely recognized that biomass burning emissions are a major source of tropospheric gas and aerosol pollutants. Galanter et al (2000) estimated that biomass emissions account for 15 to 30% of the entire tropospheric CO background. Biomass emitted CO is about twice that from fossil fuel combustion on the global scale (Holloway et al 2000). Biomass burning is also an important source of aerosols.

The TRACE-P field experiment was performed with two aircrafts (NASA DC8 and P3B) from early March to early April of 2001, a traditional season of biomass burning in Southeast Asia. During the TRACE-P period, aircraft measurements indicated that biomass emission was a big contributor to CO, black carbon (BC), organic carbon (OC), and HCN in this region. Satellite images also showed that fires frequently appeared in Southeast Asia; and synoptic weather reports recorded frequent “haze” weather, a

signal of biomass smog. The strong biomass influence in this region is not only identified by TRACE-P experiment, but also by previous experiments (Maloney et al 2001).

It is difficult to quantify the biomass influences directly through measurements alone. East Asia is the most populous region in the world, and is also largely a main developing region. This region has very high anthropogenic emissions, in which biofuel emissions play a large role (Woo et al, this issue). Since the burning materials are similar, it is not easy to distinguish the biomass and biofuel pollutants just based on chemical analysis. In fact, it is also not easy to divide the contribution of biomass burning from fossil fuel burning, because most of the plumes observed by TRACE-P aircrafts contain mixtures of emission sources. Three-dimensional models can help evaluate the biomass influences for this period.

In this paper, we use a three-dimensional model to simulate the role of biomass burning, and compare to the TRACE-P measurements and some surface station data. Based on these simulations, we evaluate the direct and indirect influences of biomass burning on TRACE-P flights and on the region as a whole.

2. Methodology:

We employed the STEM 2K1 (Tang et al, this issue) regional chemical transport model to make simulations for this period. The STEM model has a detailed chemical mechanism (SAPRC 99) and explicit photolysis solver (NCAR Tropospheric Ultraviolet-Visible radiation model). This model was successfully used for TRACE-P simulations and calculated values compared well with the observed data (Carmichael et al, this issue; Tang et al, this issue). The biomass emissions used in this study are described in Woo et al (this issue). Streets et al. (this issue) describe our anthropogenic emissions in detail.

For this study, we performed two simulations: one with and another without biomass emissions, named NORMAL, and NOBIOM, respectively. The NORMAL simulation is our baseline run, and considers all emissions, deposition, gas-phase chemistry, transport, diffusion, and aerosol influences on photolysis rates. This simulation is the same as the baseline simulation presented in Tang et al (this issue) and Carmichael et al (this issue). In this study, we did not consider the role of heterogeneous reactions on aerosol surfaces. The NOBIOM simulation is the same, except the emissions from open burning sources were set to zero.

3. Biomass CO identified by observations and simulations

CO is an important species to represent the evidence of biomass burning, since this species has a large biomass-emission source, and can be transported over long distances. Figure 1 shows the estimated total biomass CO emission rate (Woo et al, this issue) of Southeast Asia, including Burma, Thailand, Vietnam, Laos and Cambodia, derived from fire count information. Biomass burning emissions are highly uncertain, and must be evaluated. Since the strongest impacts of biomass burning are in the source areas, we choose that area for the emissions evaluation. Figure 1 shows the comparisons of CO concentrations at four Thailand regional stations, located in the north of Thailand. The NORMAL simulation agrees well with the surface measurements, and successfully captured the biomass CO peak on March 8th (the 67th Julian day). The differences between the NORMAL and NOBIOM simulations indicate that the contribution from biomass CO is as high as 3ppm. The biomass CO emission in this region reached a maximum on March 7th. The CO concentration peaked one day later, as indicated by both the modeled and observed results.

The strong biomass burning emissions from Southeast Asia can have large influence on the TRACE-P aircraft measurements. By comparing model results with the aircraft data, we identified 9 flight periods

where the biomass signals were significant, as shown in Figure 2. Figure 2 indicates that the NORMAL simulation agrees well with the observed CO concentrations, and the NOBIOM results significantly underestimate CO concentrations for these 9 flight segments. The corresponding biomass CO horizontal distributions, wind fields, and flight paths are presented in Figure 3 at the major altitudes of these flights.

From March 7th to 10th, a cold front was the main weather activity in this region. Five TRACE-P flights sampled the evolution of this front during this period. The frontal wind system transported the biomass and anthropogenic pollutants from west to east, and formed a clear band with high-concentration of pollutants. Most biomass pollutants were exported to the west along the warm conveyor belt associated with this front. Behind this front, the high-pressure system brought clear air from high altitude to the lower layer, and generated a large CO gradient across the front. The five TRACE-P flights (P3 flight 9, 10, 11, and DC8 flight 7, 8) encountered the strongest biomass CO plumes. As shown for P3 flight 9 (Figure 2), the biomass CO contribution was up to 200ppbv, which nearly doubled the background CO concentrations at some locations. This feature was also captured in a similar altitude range (from 2km to 6km) by the DC8 flight 7. Our trajectory analysis points out that the high CO concentrations of both the P3 flight 9 and DC8 flight 7 came from Southeast Asia after traveling 2 to 3 days.

On March 9th, the cold front moved to 20N. As shown in Figure 3, both the P3 flight 10 and the DC8 flight flew along the 20N latitude line, with a purpose to observe the continental outflow brought by the front. Figure 2 shows that biomass CO heavily influenced the P3 and DC8 flights at these times. This biomass influence concentrated in the layers from 2km to 4km. This situation implies that the airmasses below and above 2km may come from different sources. Our backward trajectory verifies this fact. Due to the complex frontal structure and stratification, the airmass was clearly divided, with airmasses arriving at 2 to 4km coming from Southeast Asia, and the airmasses below 2km coming from northern China. The biomass airmass from 2 to 4km altitudes departed from northern Thailand on about March 7th when the

biomass emissions in Southeast Asia reached the maximum. The absolute CO concentration at that departing location was about 800ppbv. Although this concentration is much lower than the peak concentration appearing in the same location one day later, as shown in Figure 1, it still contributed significant CO enhancements along the aircraft flight paths.

On March 10th, the cold front nearly disappeared. The purpose of this flight was to measure the airmass of the marine boundary layer. This flight encountered some aged biomass airmasses at low altitudes. Our analysis shows that that low-altitude biomass airmass did not come from Southeast Asia directly, but stayed over the East China Sea for more than 5 days. Although the biomass airmass is very aged, its CO signal is still sufficiently strong to affect the CO concentrations.

On March 13th, there was another cold front that passed along 20N. The biomass airmass encountered by the P3 flight 12 was also transported along the warm conveyor belt of the front. The transport situation is similar to that on March 9th, and the high biomass CO also appeared at the altitude of ~ 3km. However, the flight path was different. The flight path crossed over the front line, and entered the post-front high-pressure system. The biomass signals lasted only 1 hour, in the P3 back-and-forth flight path.

Both P3 flight 13 and DC8 flight 11 encountered significant biomass CO signals on March 17th over the East China Sea and the western Pacific Ocean. A weak cold front existed and extended from the northeast to Taiwan, but its influence on the flights was not strong. This situation was a typical monsoon-driven transport system. The prevailing southwest monsoon transported biomass airmass in the northeast direction from the surface to about 4km. Biomass burning affected nearly the entire P3 flight 13, and contributed a CO enhancement of about 50ppbv. The biomass-affected area was quite broad, and covered nearly the entire western Pacific from 15N to 40N. Biomass burning provided an enhanced “background”

of CO concentration to this region. This background overlapped with the Shanghai plume, as indicated by the P3 observation.

The P3 flight 17 encountered a typical low-altitude aged biomass airmass on March 27th. The original purpose of this flight was to measure the volcanic plume emitted from Mt. Miyakajima. So this flight kept a low altitude (mostly below 500 meter). Although the NORMAL simulation underestimated the CO concentration at some locations, the widespread biomass burning influence contributed about 50ppbv of CO to the background.

4. Observed Biomass Features

The TRACE-P flight paths are far way from the biomass source region. Our trajectory analysis indicates that the biomass airmasses take at least two days to arrive at the aircraft locations during these scenarios. On its transport way, the biomass plume may also mix with other emissions, since other sources in the region are also strong. Even though the model and observations clearly identified the biomass CO signatures in the flights mentioned above, the biomass features sometimes are still not strong enough to be distinguished from background and other influences. Here we resample the nine flight periods with simulated biomass CO. When the biomass CO concentrations are higher than 60ppbv, we define the scenarios as "biomass events", which includes about 140 data points in 5-minutes merged dataset. We define all TRACE-P scientific flight periods other than the 9 biomass-affected periods as "other events" for comparison purpose.

Figure 4 shows the observed correlations of CO versus HCN (Hydrogen Cyanide), K^+ (potassium), NO_y and C_2H_2 (ethyne) during biomass and other events. The observed HCN is only available for DC-8 flights

(Singh et al, this issue), and the other species in Figure 4 were observed by both aircrafts. These species have relatively long lifetimes, so we can use this information to examine the original emission signals.

The biomass airmasses tend to have higher $\Delta HCN/\Delta CO$ and $\Delta K^+/\Delta CO$ ratios, and lower $\Delta NO_y/\Delta CO$ and $\Delta C_2H_2/\Delta CO$ ratios than the airmasses from other sources (mainly anthropogenic emissions). The slopes of HCN versus CO are 0.0015 for biomass events and 0.0011 for other events. This biomass slope is much higher than that measured in biomass plumes in Australian tropical savannas during the 1991 and 1992 dry seasons by Hurst et al (1994), which was about 0.00028. This difference reflects regional differences in the biomass burning characteristics. The biomass $\Delta K^+/\Delta CO$ slope (0.0038) is also higher than that measured over the Indian Ocean, 0.0029, by Reiner et al. (2001). Reiner et al. (2001) mentioned that their samples might contain both biomass and biofuel signals. Since the biomass events that we define here are the very strong scenarios of biomass burning, it is possible that the India and Southeast Asia have similar K^+/CO biomass emission ratios. The biggest slope difference between biomass and other events are seen for the values of $\Delta NO_y/\Delta CO$, and the slope in the other events is about 3 times that in the biomass events. Hurst et al (1994) reported that the $\Delta NO_x/\Delta CO$ value in savannas biomass burning was about 0.023, which is even higher than the $\Delta NO_y/\Delta CO$ slope in the other events for the TRACE-P flights. Their observed $\Delta C_2H_2/\Delta CO$ ratio was about 0.00072, which is 50 times smaller than that in TRACE-P biomass events (0.0038). The other events of TRACE-P flight have an even higher $\Delta C_2H_2/\Delta CO$ value (0.0049). It also shows that the biomass airmasses emitted from Southeast Asia have lower $\Delta NO_y/\Delta C_2H_2$ than that in the savannas biomass plumes (Hurst et al, 1994), which implies their difference on NO_x/VOC emission ratio.

These results indicate that the biomass burning in Southeast Asia and Australian tropical savannas belong to different types. Australian tropical savannas are relatively dry, and have higher burning temperature, and the burning is relatively complete. These conditions benefit the production of nitrogen oxidants, but

reduce the emission rates of VOC (volatile organic compound) and HCN. The biomass burning in Southeast Asia represents a contrary situation. This region in the monsoon season is very humid, and the combustion efficiency in tropical forests should be relatively incomplete. The TRACE-P observations show that these biomass plumes contain very low nitrogen oxidants, but are rich in VOCs. The airmass characteristics bring a totally different regional O_3 producing scenario. NO_z (NO_y-NO_x) is the oxidized products of NO_x, including peroxyacetyl nitrate (PAN), HNO_3, HNO_2 et al. The ratio O_3/NO_z represents the upper limit of the ozone production efficiency (OPE) per unit NO_x (Trainer et al., 1993). Figure 4 shows that the $\Delta O_3/\Delta NO_z$ value (17.55) in the biomass events is 10 times as that value (1.734) in other events. The biomass airmasses emitted from Southeast Asia have extraordinary high OPE.

5. Other Biomass Influences on TRACE-P flights

The influence of biomass emissions on gas-phase chemistry of this region can be divided into two parts: the influence via radiative forcing, and the non-radiative influence. Tang et al. (this issue) found that BC and OC aerosols impose a significant impact on regional radiation transfer, and reduce primary photolysis rates by up to 60% in low altitudes. This impact further affects regional photochemistry. The biomass burning are the main supplier of BC and OC in south of 30N in this region. To distinguish the biomass burning influences due to radiative effects, we ran another simulation that was the same as the NORMAL case, but without biomass aerosols (we call this the "NOBAOD"). The difference between NORMAL and NOBAOD represents the biomass influence via photolysis processes, the difference between NOBAOD and NOBIOM represents the biomass non-radiative influence, and the difference between NORMAL and NOBIOM shows the net biomass influence.

Figure 6 shows the biomass influences on $J[NO_2]$ (NO_2 photolysis rate), OH, HO_2, and O_3 plotted against the biomass contribution to CO during the selected 9 biomass-affected periods. The $J[NO_2]$ reduction is

not due to CO enhancement, but due to biomass aerosols in these biomass-affected periods. Biomass aerosols contain black carbon (BC), organic carbon (OC) and potassium, and these particles are co-emitted and transported with gaseous compounds. The concentrations of biomass aerosol are usually proportional to biomass CO, and emission factors for biomass burning are often referenced to CO. The existence of biomass aerosols can affect the photolysis rates below and above them. Since the biomass aerosol contains BC, it is strongly radiatively absorptive, and causes the J-values to decrease (Tang et al. this issue). The observed data of aerosol single scattering albedo (SSA) show high variability. The average value of observed SSA was 0.821 for the selected 9 biomass-affected periods, and the NORMAL simulation yielded a value of 0.828, and the NOBIOM simulation had a value of 0.839. In strong biomass burning events, the SSA change due to biomass aerosol is higher. Figure 5 shows the correlations between SSA and aerosol optical extinction coefficient (AOE) during the biomass events, as defined in section 4. The NORMAL simulation slightly overestimated the aerosol absorption, and caused an underestimation of SSA. The simulation without biomass burning significantly overestimated SSA by missing some low SSA values.

The effect on photolysis processes is not only caused by local aerosols, but also by the aerosol loadings below or above that arise from other sources. As a result, the $J[NO_2]$ reduction sometimes is not directly proportional to local biomass aerosol loading. From Figure 6, we can see that the existence of biomass aerosol generally causes $J[NO_2]$ to decrease. Other J-values, e.g. $J[O_3 \rightarrow O_2+O^1D]$, behave in a similar manner. Since OH is highly sensitive to $J[O_3 \rightarrow O_2+O^1D]$, OH decreases due to biomass aerosols. The CO and VOC enhancements due to biomass emissions can also cause an OH reduction through the reaction:

$$CO\ (R{\cdot}H) + OH + O_2 \rightarrow HO_2\ (RO_2) + CO_2\ (H_2O) \qquad (1)$$

Here we use R·H to represent the general form of VOC in photochemical reactions, and R represents alky radicals. The CO and VOC have a similar impact on OH reactions and photochemically production of O_3, though VOC reactions are more complex and need several steps to complete. When we exclude the radiative impact, reaction (1) becomes the main influence of biomass airmasses on OH, and contributes to OH reduction. Figure 6b shows that sometimes OH concentrations increase under the biomass non-radiative influence. The reason is that biomass CO and VOC increase O_3 levels in aged biomass airmasses, and this O_3 contributes to the OH production via:

$$HO_2\ (RO_2) + NO \rightarrow NO_2 + OH\ (RO) \qquad (2)$$

$$NO_2 + h\nu \rightarrow NO + O^3P \qquad (3)$$

$$O^3P + O_2 \rightarrow O_3 \qquad (4)$$

$$O_3 + h\nu \rightarrow O_2 + O^1D \qquad (5)$$

$$O^1D + H_2O \rightarrow 2OH \qquad (6)$$

If reactions (1) to (6) perform thoroughly, there should be a positive OH budget. However, these reactions are constrained by the NO_x availability and J-values. After long-distance transport, the biomass airmasses usually have low NO_x concentrations, and reaction (1) overwhelms the other reactions, causing OH to decrease in the aged biomass plumes. Our analysis shows that most of the OH enhancements due to the non-radiative influence in Figure 6b occur at about 2:00PM local time, when the O_3 production and J-values reached their maximum values.

Under the biomass non-radiative influence, HO_2 increased (Figure 6C) due to reaction (1). When adding the radiative influence, HO_2 sometimes decreased due to radiative-reduced OH. So the net biomass influence on HO_2 is determined by the biomass CO concentration and J-value changes due to biomass aerosols. In most of the 9 biomass-affected flight segments, the former influence was stronger.

Reactions (1) to (4) show how biomass CO and VOC leads to increases in O_3. It should be noted that most O_3 enhancements in Figure 6D are not due solely to local O_3 production increases. These O_3 enhancements are accumulated along the transport journey of the biomass airmasses, since O_3 is also a relatively long-lived species. Also because of the long lifetime, the O_3 enhancement remains in well-aged biomass airmasses. As shows in Figure 3, biomass burning provided a wide-range of CO enhancements in East Asia. These plumes have higher OPE and are NO_x limited. In Asia, biomass plumes often pass over regions with significant NO_x emissions, and thus O_3 production can be sustained for long periods. The TRACE-P flights captured the signal of regional O_3 enhancement due to biomass burning. Figure 6D shows that the biomass radiative influence restrains O_3 production, and sometimes turns the net biomass influence on O_3 to negative. It also implies that reaction (3) is stronger than reaction (5) in the lower troposphere, since J-value reduction mostly leads to O_3 reduction. Overall, the impact of biomass aerosols on O_3 via affecting photolysis rates is much weaker than the biomass influence on O_3 due to direct reactions, as indicated by the small slope difference of Figure 6D.

6. Biomass Regional Influences

The discussions above focused on the influences of biomass burning on trace gases measured along the TRACE-P flight paths. Figure 2 presented 6 scenarios of biomass CO outflows during this period. Tang et al (this issue) show the aerosol influences on J-values, OH, and O_3 in regional scale. In that paper, most aerosol influences south of 25N are due to biomass burning. Our analysis shows that both radiative and non-radiative influences of biomass burning are concentrated in the layer below 4km. Most biomass signals captured by TRACE-P flights also appeared in these layers.

Figure 7 shows the simulated March-averaged net biomass influences on daytime OH, HO_2 and HCHO below 1km and from 1 to 3km. On average, the OH decrease due to biomass influence is as great as 40% below 1km, and up to 35% from 1 to 3km. The biggest OH decrease occurs not in the biomass burning areas, but in the downwind locations. The background OH in Southeast Asia is low because this region also has strong biogenic emissions. Under these conditions, reaction (1) becomes weak, and the biomass non-radiative influence on OH becomes positive. In this region, the biomass non-radiative influence can enhance OH concentrations by up to 90%. In the downwind regions, where the biogenic emissions are not so strong during this season, the biomass non-radiative influence on OH turns to negative. The biomass aerosol influence always leads to reduced photolysis rates and OH. This influence is mainly determined by the biomass aerosol optical depth, and appears the strongest in the biomass burning areas. Our analysis indicates that in Southeast Asia, the non-radiative and radiative influences are of the same order of magnitude. Downwind, the radiative influence is usually much stronger than the non-radiative influence on OH, and both of them lead to decrease OH concentrations. On average, the radiative influence on OH is stronger than the non-radiative effects. The net biomass influence on OH, combined by both of these influences, mainly exists south of 35N, and becomes weak with height (Figure 7).

The biomass influence on HO_2 has some features similar to OH. Our analysis shows that the biomass non-radiative influence on HO_2 is positive. The radiative influence on daytime HO_2 is always negative, since the influence on OH is also negative. The net biomass influence is determined by the strengths of these two components, and has a geographic distribution similar to that of OH. The net influence on HO_2 is positive in most biomass burning areas except in northern Thailand, and becomes negative in most downwind areas. In the horizontal direction, the biomass non-radiative influence on HO_2 decays faster than the radiative influence along the transport route. In the vertical direction below 3km, the biomass non-radiative influence decays slower than the radiative influence along the vertical enhancement. The difference between these two influences reflects the following fact: the non-radiative influence is mainly

determined by the local chemical compound's concentrations, and the radiative influence mostly depends on the aerosol optical thickness. The radiative influence is more sensitive to altitude change than the non-radiative influence since the biomass plume can elevate up to the middle troposphere, and the latter is more sensitive to the dilution of biomass compounds than the former. On the regional average, these two influences on HO_2 are of the same order of magnitude.

Our sensitivity study shows that both non-radiative and radiative influences of biomass burning contribute to increasing formaldehyde (HCHO) concentrations. The reason that the non-radiative process increases formaldehyde is because biomass burning also emits significant amounts of VOCs, and HCHO is one of the main products of VOC oxidation. In biomass burning regions, the HCHO production is very high. It should be noted that the background HCHO in Southeast Asia is also high due to strong biogenic emissions, and this is identified by the GOME (Global Ozone Monitoring Experiment) satellite observation (see website: http://wwws.harvard.edu/chemistry/trop/tracep/hcho_tp.jpg). Under these conditions, the photolysis processes mainly lead to HCHO destruction. So reducing J-values results in higher HCHO concentrations, and the biomass radiative influence on HCHO appears positive. This radiative influence is usually weaker than the non-radiative influence. For example, in the altitude below 1km, the non-radiative process can enhance HCHO up to 55%, and the radiative influence contributes to HCHO increase up to 20%.

Reactions (3) and (4) are the main sources of photochemically generated ozone. So, reductions of J-values lead to O_3 decreases. Figure 8 shows that biomass aerosols can reduce O_3 by up to 5 ppbv below 1km, and 3ppbv from 1 to 3km by reducing J-values. The biomass non-radiative process can cause O_3 enhancements of more than 10ppbv in the layers below 3km. The biomass influences on low-layer O_3 also depend on the NO_x concentrations. In the strong biomass plumes that mix with few other airmasses, the NO_x/VOC and NO_x/CO ratios were very low, but OPE is very high The widespread biomass plumes

usually mix with some high-NO_x anthropogenic pollutants. So, in general, the O_3 production caused by biomass burning was not constrained by NO_x availability, and the biomass non-radiative influence on O_3 keeps positive. Carmichael et al. (this issue) indicated that as a region with low NO_x/VOC ratio, Southeast Asia is more sensitive to NO_x increase than to VOC increase for O_3 enhancement. In most places, the biomass net influence on O_3 is also positive. Only in the middle and lower reaches of the Yangtze River, including Shanghai, does the biomass net influence turn to be slightly negative in the layer below 1km. As a populous region, the Yangtze River surrounding areas have very high anthropogenic emissions. Compared to these strong local emissions, the biomass CO and VOCs transported from Southeast Asia become insignificant, especially in Shanghai plume. Under that circumstance, the influence of biomass aerosols on photochemical processes may be slightly higher than the biomass non-radiative O_3 production. On a regional average, the biomass non-radiative influence on O_3 is much higher than the radiative influence. For March, the biomass burning causes an O_3 enhancment band in South of 30N, where the O_3 concentration increases generally by more than 2 ppbv, and occasionally by up to 15 ppbv (Figure 6D). Our study shows that this enhancement can extend up to 8km altitude along the transport route.

7. Conclusion

This study used the three-dimensional chemical model, STEM2K1, to retrieve the impacts of biomass burning in East-Southeast Asia during the TRACE-P period. By using CO as the main indicator, the modeled results agree with both surface observations and TRACE-P airborne measurements. The sensitivity study enabled us to identify 9 periods with significant biomass influences from a total of 24 TRACE-P flights. Through studying these 9 scenarios, we described the main features of biomass CO outflow from Southeast Asia. In this outflow, the biomass burning forms a widespread region where the CO concentrations are enhanced by more than 30ppbv. In the warm conveyor belt of frontal systems, the

exported biomass CO concentration can reach up to 500ppbv. Among the 9 biomass-affected scenarios, 8 were associated with frontal activities.

Using these simulations, we sampled the biomass signals quantitatively. Through analyzing the observed data in the biomass events, the characteristics of the biomass airmasses from Southeast Asia were identified. The Southeast Asia biomass airmasses contains fewer nitrogen oxidants, but larger amounts of HCN and NMHC (non-methane hydrocarbon). The biomass ratios are higher on $\Delta HCN/\Delta CO$ (0.0015), and $\Delta C_2H_2/\Delta CO$ (0.0036), and lower on $\Delta NO_y/\Delta CO$ (0.005) than those reported from Australian tropical savannas fire (Hurst et al. 1994).

Biomass burning imposes complex influences on regional tropospheric chemistry, which can be divided into radiative and non-radiative influences. The complexity arises even more when the biomass plumes interact with biogenic and anthropogenic emissions. Due to the low OH background constrained by the strong biogenic emissions, the biomass gas-phase compounds mainly contribute to OH production consumption in Southeast Asia. Our analysis showed that the biomass non-radiative processes also increase the HO_2, HCHO, and O_3 concentrations in the lower troposphere. The biomass radiative influences contribute to OH, HO_2, and O_3 reduction, but increased HCHO concentrations by reducing its photolytic loss. Arranged by the sensitivity to the J-value change caused by biomass aerosols, we found that $OH > HO_2 > HCHO > O_3$ in regional average. Averaged over March, the biomass burning net influences reach up to 50% for OH, 40% for HO_2, 60% for HCHO, and 10 ppbv for O_3 below 1km. These highest influences usually appear in biomass burning areas or their adjacent downwind sites.

These results confirm the impact role that biomass burning plays in the chemistry and pollutant outflows in Asia. These results also point out the need to take into account both aerosol and gas-phase chemical

processes. These findings underscore the need to further quantify and refine our estimate of biomass burning emissions.

Acknowledgements:

This work was supported by NASA GTE TRACE-P, ACMAP, and NSF Atmospheric Chemistry program. The Thailand surface data were collected by Air quality and Noise Management Division, Pollution Control Department, Ministry of Natural Resources and Environment, Thailand.

References:

Carmichael, G. R., Y. Tang, G. Kurata, I. Uno, D. G. Streets, J.- H. Woo, H. Huang, J. Yienger, B. Lefer, R. E. Shetter, D. R. Blake, A. Fried, E. Apel, F. Eisele, C. Cantrell, M. A. Avery, J. D. Barrick, G.W. Sachse, W. L. Brune, S. T. Sandholm, Y. Kondo, H. B. Singh, R. W. Talbot, A. Bandy, A. D. Clarke, and B. G. Heikes, Regional-Scale chemical transport modeling in support of intensive field experiments: overview and analysis of the TRACE-P Observations, , J. Geophys. Res., (this issue).

Kamm, S., O. Mohler, K. H. Naumann, H. Saathoff, and U. Schurath, The heterogeneous reaction of ozone with soot aerosol. Atmos. Environ., 33 (28), 4651-4661, 1999.

Galanter, M., H. Levy and G. R. Carmichael, Impacts of biomass burning on tropospheric CO, NO_x, and O_3, J. Geophys. Res.,105 (D5), 6633-6653, 2000.

Holloway, T., H. Levy and P. Kasibhatla, Global distribution of carbon monoxide, J. Geophys. Res., 105 (D10), 12123-12147, 2000.

Hurst, D. F., D. W. T. Griffith, and G. D. Cook, Trace gas emissions from biomass burning in tropical Australian savannas. J. Geophys. Res., 99 (D8), 16441-16456, 1994.

Maloney, J. C., H. E. Fuelberg, M. A. Avery, J. H. Crawford, D. R. Blake, B. G. Heikes, G. W. Sachse, S. T. Sandholm, H . Singh, and R. W. Talbot, Chemical characteristics of air from different source regions during the second Pacific Exploratory Mission in the Tropics (PEM-Tropics B), J. Geophys. Res., 106 (D23), 32609-32625, 2001.

Reiner, T., D. Sprung, C. Jost, R. Gabriel, O. L. Mayol-Bracero, M. O. Andreae, T. L. Campos, and R. E. Shetter, Chemical characterization of pollution layers over the tropical Indian Ocean: Signatures of emissions from biomass and fossil fuel burning, J. Geophys. Res., 106 (D22), 28497-28510, 2001.

Singh, H. B., L. Salas, D. Herlth, R. Kolyer, E. Czech, W. Viezee, Q. Li, D. J. Jacob, D. Blake, G. Sachse, C. N. Harward, H. Fuelberg, and C. M. Kiley, In-situ measurements of HCN and CH3CN in the Pacific troposphere: Sources, sinks, and comparisons with spectroscopic observations. J. Geophys. Res., (this issue).

Streets, D. G., T.C. Bond, G. R. Carmichael, S. D. Fernandes, Q. Fu, D. He, Z. Klimont, S. M. Nelson, N. Y. Tsai, M. Q. Wang, J.-H. Woo, and K. F. Yarber, A year-2000 inventory of gaseous and primary aerosol emissions in Asia to support TRACE-P modeling and analysis (this issue).

Tang, Youhua, G. R. Carmichael, I. Uno, J.-H. Woo, G. Kurata, B. Lefer, R. E. Shetter, H. Huang, B. E. Anderson, M. A. Avery, A. D. Clarke and D. R. Blake, Impacts of aerosols and clouds on photolysis frequencies and photochemistry during trace-p, part II: three-dimensional study using a regional chemical transport model, J. Geophys. Res., (this issue).

Trainer, M., D. D. Parrish, M. P. Buhr, R. B. Norton, F. C. Fehsenfeld, K. G. Anlauf, J. W. Bottenheim, Y. Z. Tang, H. A. Wiebe, J. M. Roberts, R. L. Tanner, L. Newman, V. C. Bowersox, J. F.

Meagher, K. J. Olszyna, M. O. Rodgers, T. Wang, H. Berresheim, K. L. Demerjian and U. K. Roychowdhury, Correlation of ozone with NOy in photochemical aged air. J. Geophy. Res., 98(D2), 2917-2925, 1993.

Woo, J.-H., Y. Tang, D. G. Streets, J. Dorwart, G. R. Carmichael, S. Pinnock, K. F. Yarber, G. Kurata, N. Thongboonchoo, Biomass and biogenic Emissions and their impact on trace gas distribution during TRACE-P, J. Geophys. Res., (this issue).

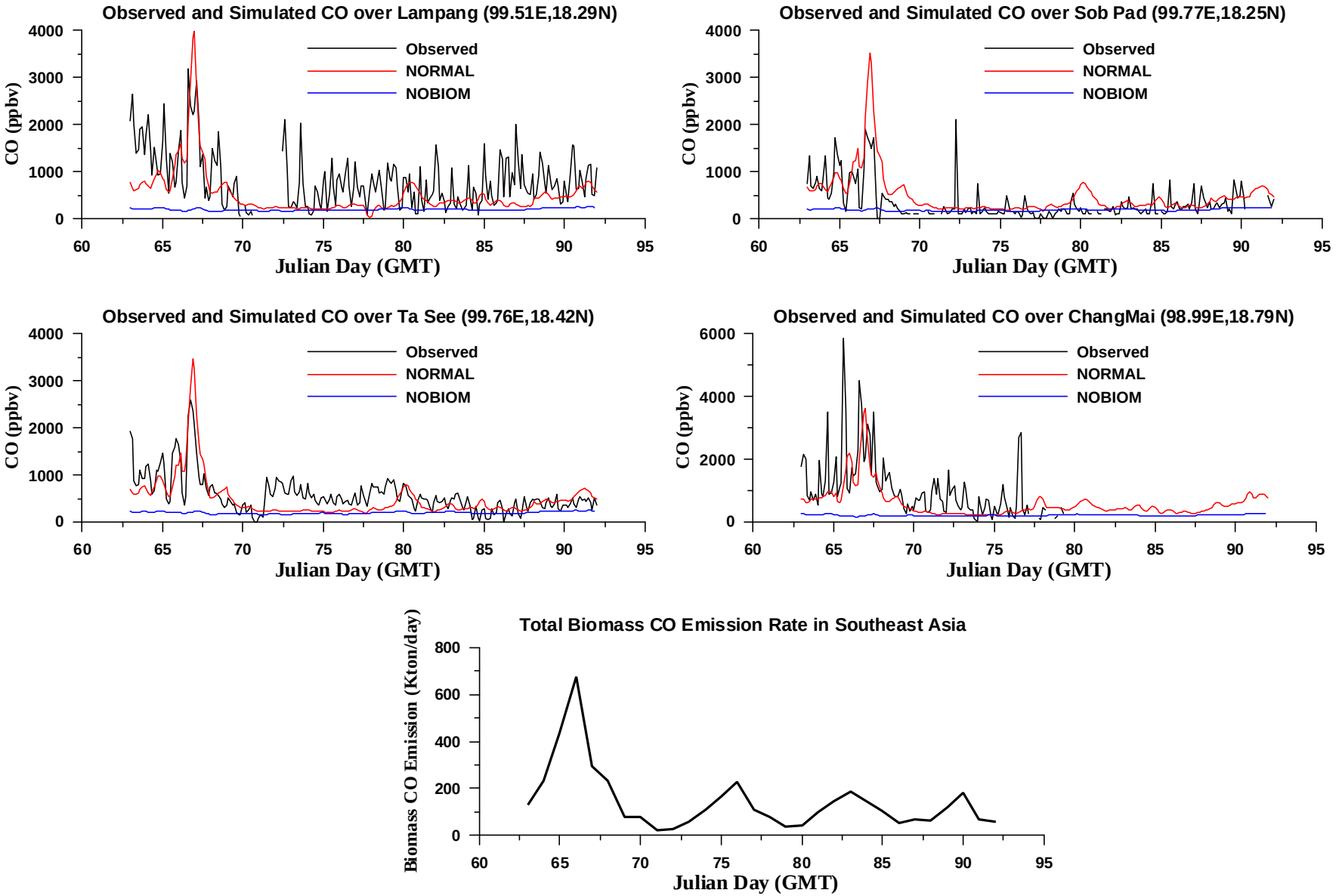

Figure 1. Observed and simulated CO concentrations over four Thailand surface stations, and estimated biomass CO emissions in Southeast Asia, during the TRACE-P period. The Lampang, Sob Pad and Ta See surface stations are located in rural sites, and the Chang Mai station is a suburban site.

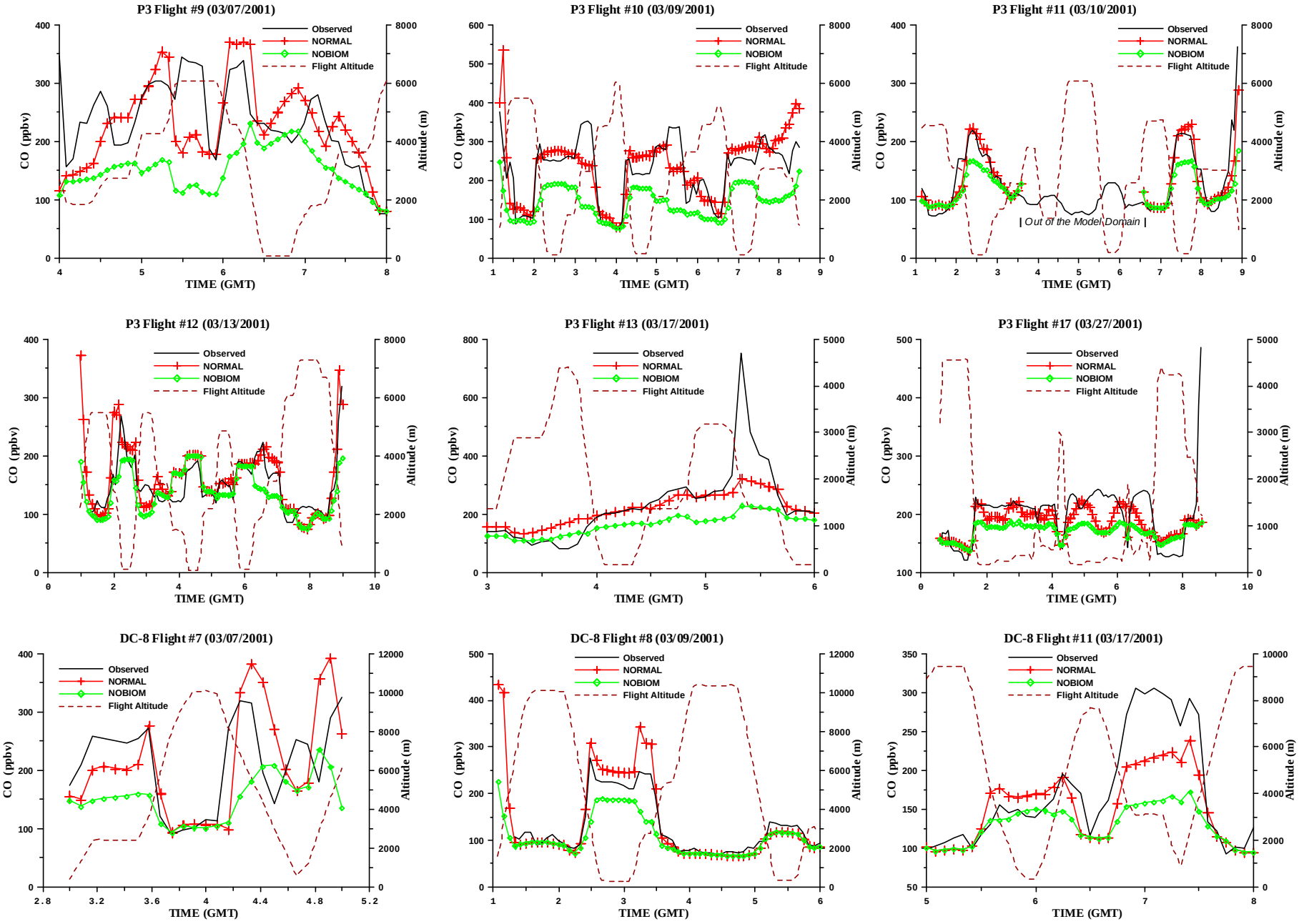

Figure 2. Observed CO compared to NORMAL and NOBIOM simulations for flight segments identified as high biomass influences

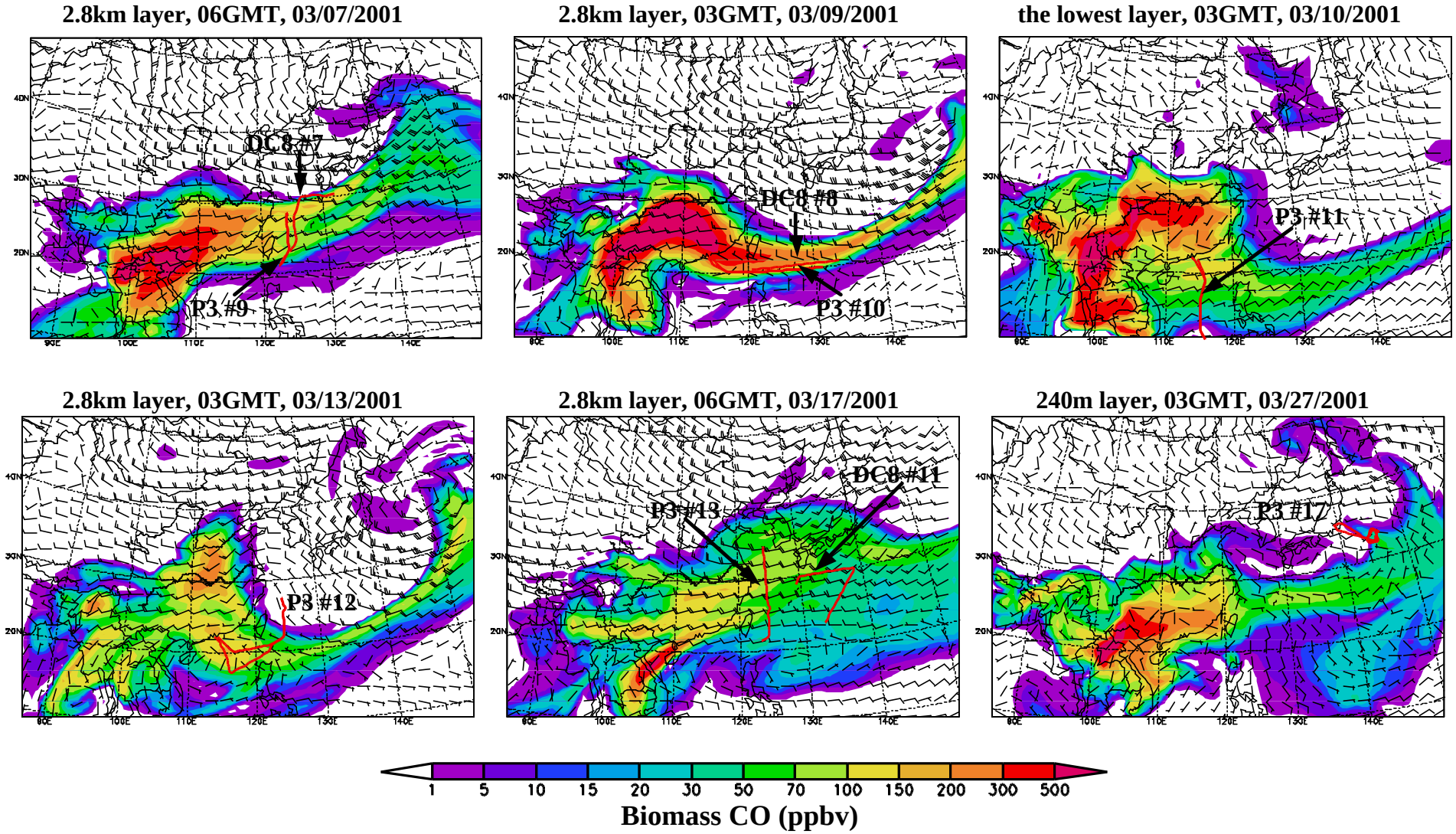

Figure 3. Simulated biomass CO concentrations at the major altitudes for the 9 flights shown in Figure 2. The red lines refer to the flight paths mentioned in Figure 2.

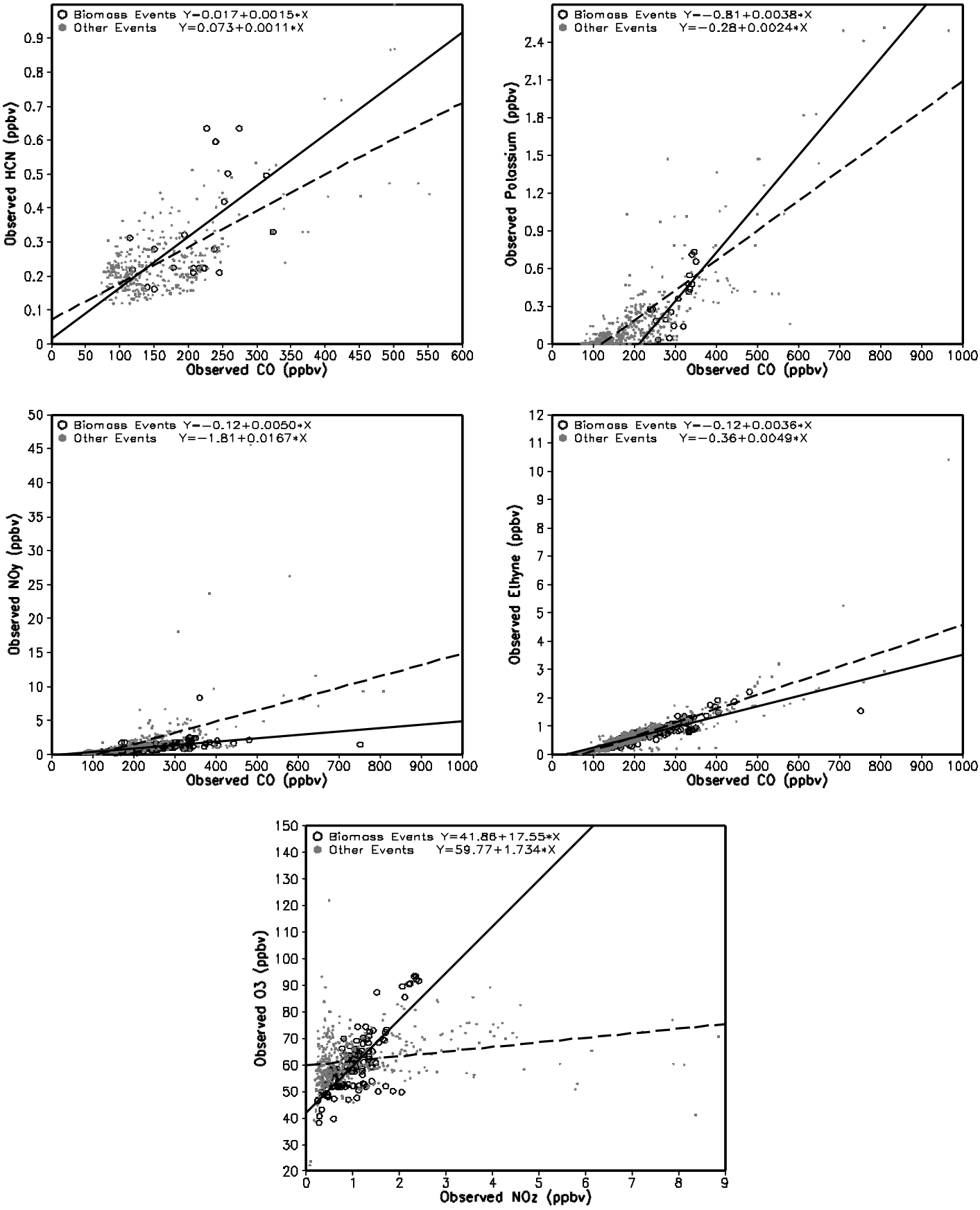

Figure 4, Observed correlations of CO versus HCN, potassium, NO_y and ethyne, and O_3 versus NO_z in biomass and other events. The open circles and solid fit lines refer to the biomass events, and the small closed circles and dashed fit lines represent the other events.

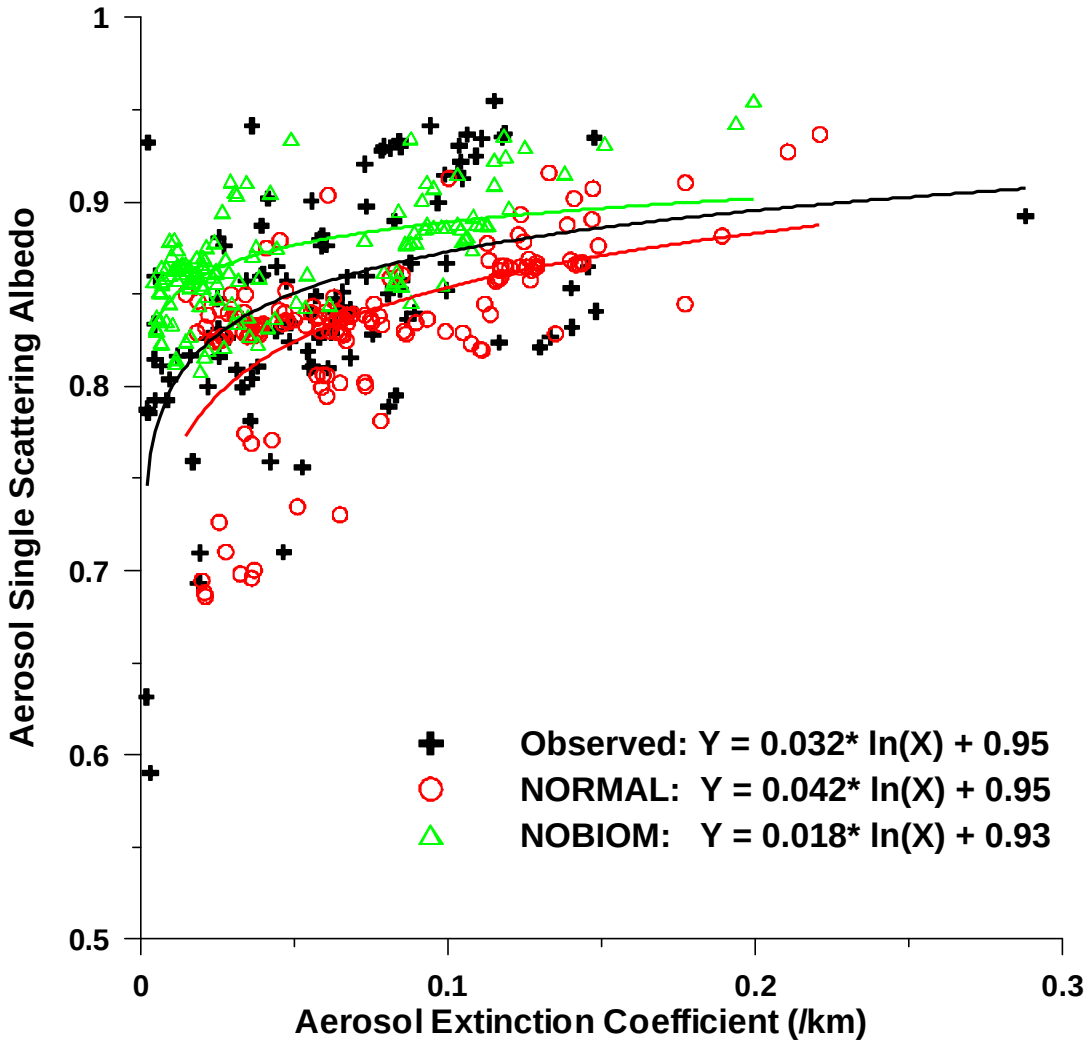

Figure 5, The observed and simulated correlations between aerosol single scattering albedo and extinction coefficient during the biomass events (biomass CO > 60ppbv).

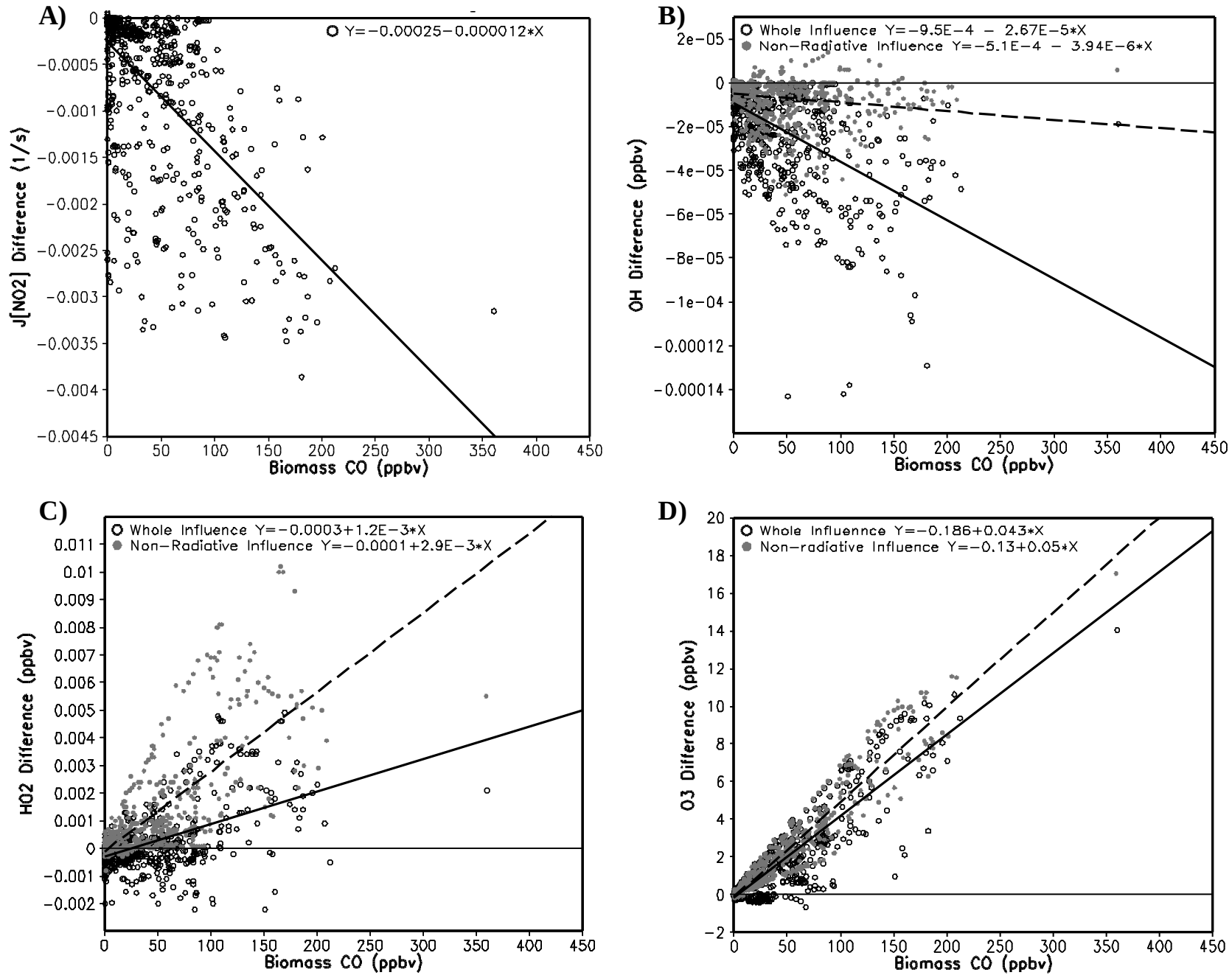

Figure 6, Simulated biomass net and non-radiative influences on J[NO_2], OH, HO_2 and O_3 versus biomass CO during the 9 biomass-affected periods of TRACE-P flights.

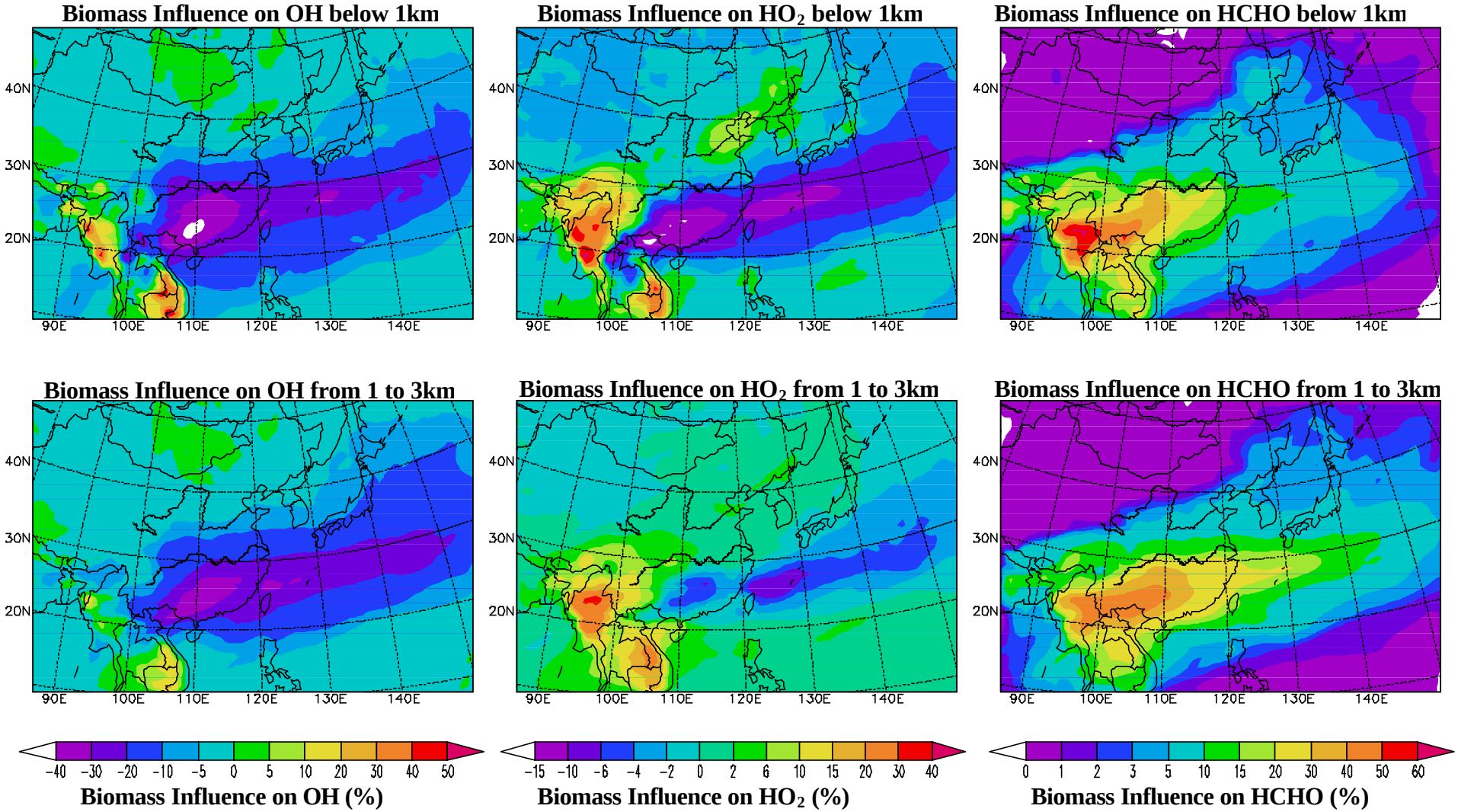

Figure 7, March-averaged biomass net influences on daytime OH, HO_2 and formaldehyde for the layers below 1km and from 1 to 3km, represented as percentage change.

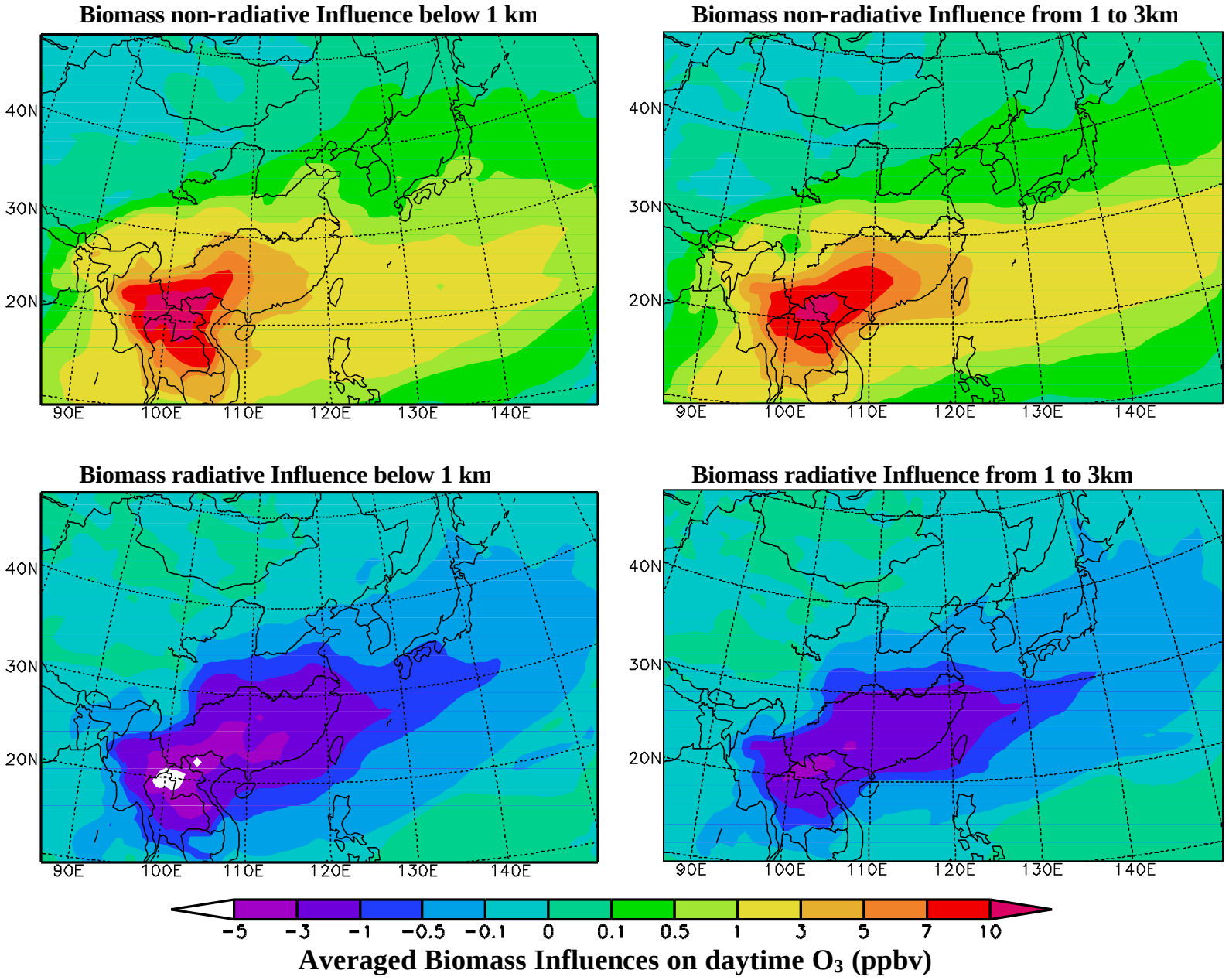

Figure 8, March averaged biomass radiative and non-radiative influences on daytime O_3 for the layers below 1km and from 1 to 3km.